Materials Today Physics 59 (2025) 101954

Contents lists available at ScienceDirect

Materials Today Physics

journal homepage: www.journals.elsevier.com/materials-today-physics

Remote spatiotemporal control of local states in thermal lattice

Quan Liu [a], Zhaochen Wang [a], Sun-Kyung Kim [b], Xiaobing Luo [a], Philippe Ben-Abdallah [c], Wonjoon Choi [d,*], Run Hu [a,b,**]

[a] School of Energy and Power Engineering, Huazhong University of Science and Technology, Wuhan, 430074, China
[b] Department of Applied Physics, Kyung Hee University, Yongin-Si, Gyeonggi-do, 17104, Republic of Korea
[c] Laboratoire Charles Fabry, UMR 8501, Institut d'Optique, CNRS, Universit e Paris-Saclay, 2 Avenue Augustin Fresnel, Cedex, 91127, Palaiseau, France
[d] School of Mechanical Engineering, Korea University, Seoul, 02841, Republic of Korea

ARTICLE INFO

Keywords:
Remote spatiotemporal control
Local thermal state
Thermal insulation
Thermal synchronization

ABSTRACT

The ability to actively control local states in thermal lattice provides critical insights into nonequilibrium thermodynamics and enables novel approaches to energy management across nano to macroscopic scales. The process of thermalization in thermal lattice is a kind of neighboring interactions due to the media- and path-dependent characteristic of Fourier's diffusion, rendering the significant challenge for remote control of local thermal state. Here we construct the time-independent Hamiltonian of a thermal lattice system with consideration of conduction and convection simultaneously and derive the optimal external command for active control of local thermal states. We implement three thermal targeting control—insulation, synchronization, and fluctuation—by modulating power inputs and precisely monitoring temperature evolution to demonstrate the validity and powerfulness of remote spatiotemporal control of local thermal states. Our work paves the way for remote spatiotemporal control of thermal states and provides efficient alternatives for advanced active thermal management in complex architectures.

1. Introduction

Controlling thermal states offers fundamental insights into nonequilibrium thermodynamics in interacting thermal lattice. It establishes a direct connection between a system's thermal trajectories during relaxation and the external physical constraints imposed upon it. Moreover, it provides a means to relate the system's dynamical evolution to its fundamental limits in heat exchange [1,2] and energy dissipation [3]. Precise thermal regulation is particularly critical in thermally sensitive platforms such as quantum processors [4], mechanical metamaterials [5,6] and biological sensors [7,8]. It further supports the development of thermal logic gates and memory elements, forming the foundation of thermal information processing [9]. Local temperature control enhances the stability and operational lifetime of materials and devices [10]. In energy harvesting systems, directed heat flow significantly increases power output. Additionally, thermal control aids in synchronizing coupled processes in complex architectures, ensuring coherent and reliable operation [11–13].

However, the manipulation of heat diffusion has been long considered not as flexible as electromagnetic waves [14] as illustrated in Fig. 1(a), since the latter can be remotely controlled without media. In contrast, heat diffusion is a kind of neighboring interactions due to the media- and path-dependent characteristic of Fourier's law [15–17]. By analogy to Hamiltonian in quantum physics [18–20], local thermal states can be manipulated spatiotemporally with topological anti-Hamiltonian properties [21], enabling many intriguing phenomena such as thermal nonreciprocity [22–25], non-Hermitian skin effect [26], anti-parity-time symmetry [27] and topological edge states [28–32] etc. Thus, via some approximate external commands, active control of local thermal states has garnered increasing attentions not only for revealing the rich topological physics but also for developing related technologies for active thermal management [33]. If so, we can control local thermal states with target temperature for local heating or cooling, either with invariant temperature for thermal insulating states and thermal protection, or with customized time-varying temperature for dynamic thermal management. A recent theoretical attempt has shown a general framework for controlling thermal states in classical many-body systems via thermal radiation theoretically [34]. Yet, such remote control of

* Corresponding author.
** Corresponding author. School of Energy and Power Engineering, Huazhong University of Science and Technology, Wuhan, 430074, China.
E-mail addresses: wojchoi@korea.ac.kr (W. Choi), hurun@hust.edu.cn (R. Hu).

https://doi.org/10.1016/j.mtphys.2025.101954
Received 27 September 2025; Received in revised form 16 November 2025; Accepted 24 November 2025
Available online 25 November 2025

local thermal states has not realized experimentally.

In this work, we construct the time-independent Hamiltonian of a thermal lattice system with consideration of conduction and convection simultaneously and derive the optimal external command for active control of local thermal states. By applying the external power command to specific site, we present proof-of-concept demonstration with thermal insulation and thermal synchronization of local states in a thermal lattice system composed of solid elements interacting cooperatively via both conduction and convection numerically and experimentally. Furthermore, we demonstrate the remote control of thermal fluctuation for different sites. We offer a general protocol for controlling local states in thermal lattices that has never been directly accomplished so far with potential for accurate dynamic thermal management.

2. Derivation of Hamiltonian and optimal control protocol

To implement remote spatiotemporal control of local thermal states, we construct a thermal lattice model with N sites, both thermal energy exchange at each site through heat conduction with its neighbors and through thermal convection with the ambient thermal bath at temperature T_b as illustrated in Fig. 1(c). All the local thermal states namely the temperature evolutions $\boldsymbol{T}(t) = [T_1(t), T_2(t), \ldots, T_N(t)]^{\dagger}$ with time t are what we mainly concern here. A typical illustration of remote spatiotemporal control can be easily understood that we inject the site- and time-dependent thermal power at an arbitrary site i within the reachable domain and control the local thermal state at the target site j across the unreachable domain. Such unreachable domain can be understood as out-of-reach region such as encapsulated or isolated scenarios, and we can only control their thermal state remotely from the accessible reachable region, which is the exact necessity and significance of developing the remote control of thermal states. In our study, as all the sites are coplanar and around room temperature, we neglect the thermal radiative transfer in the system, and only consider the heat conduction and natural convection. As a result, the heat transfer in the thermal lattice can be modeled in a one-dimensional discretized sphere-rod model, where the spheres denote the site in thermal lattice, and the rods denotes coupling of neighboring sites. We assume all the thermophysical properties are constant, and assume each site is temperature uniform with rather small Biot number, the governing continuity partial differential equation yields

$$\partial_t Q_{i_x} = \rho C_p \partial_t T_{i_x} = -\nabla(q_{cond} + q_{conv}), \tag{1}$$

where Q_{i_x} indicates the internal heat energy at site i_x per unit volume, ρ and C_p are the density and thermal capacity of site i_x and T_{i_x} denotes the on-site temperature at site i_x. As depicted in Fig. 1(b), $q_{cond} = q_{i_x,i_x+1} - q_{i_x-1,i_x}$ is designated as the heat flux between neighboring sites due to heat conduction and $q_{conv} = h(T_{i_x} - T_b)$ represents the heat flux between site i_x and the external bath due to heat convection according to Newton's law of cooling. Thus, Eq. (1) can be rewritten as

$$\partial_t T_{i_x} = -(\rho C_p)^{-1}\left(q_{i_x,i_x+1} - q_{i_x-1,i_x}\right)/a_0 - h(\rho C_p)^{-1}(T_{i_x} - T_b)/a_0, \tag{2}$$

where q_{i_x-1,i_x} is described as the heat flux between sites i_x-1 and i_x with constant distance a_0, h denotes the convective heat transfer coefficient and T_b is defined as the environmental temperature. By assuming linear heat conduction and according to Fourier's law of heat conduction $q(x,t) = -\lambda \nabla T(x,t)$, further derivation of Eq. (2) leads to

$$\begin{aligned}\partial_t T_{i_x} = &\left[\left(\lambda_{i_x-1,i_x}/a_0^2\rho C_p\right)T_{i_x-1} + \left(\lambda_{i_x,i_x+1}/a_0^2\rho C_p\right)T_{i_x+1}\right] - \left[\left(\lambda_{i_x-1,i_x} + \lambda_{i_x,i_x+1}\right)/a_0^2\rho C_p\right]T_{i_x} \\ &-h(T_{i_x} - T_b)/a_0\rho C_p.\end{aligned} \tag{3}$$

By defining excess temperature $\theta_{i_x} = T_{i_x} - T_b$, effective thermal diffusivity $D_{i_x-1,i_x} = \lambda_{i_x-1,i_x}\left(\rho C_p a_0^2\right)^{-1}$ and thermal convection coefficient $C_{i_x} = h\left(\rho C_p a_0\right)^{-1}$, the derivation of excess temperature with respect to time at site i_x can be described as

$$\partial_t \theta_{i_x} = D_{i_x-1,i_x}\theta_{i_x-1} + D_{i_x,i_x+1}\theta_{i_x+1} - \left(D_{i_x-1,i_x} + D_{i_x,i_x+1} + C_{i_x}\right)\theta_{i_x}, \tag{4}$$

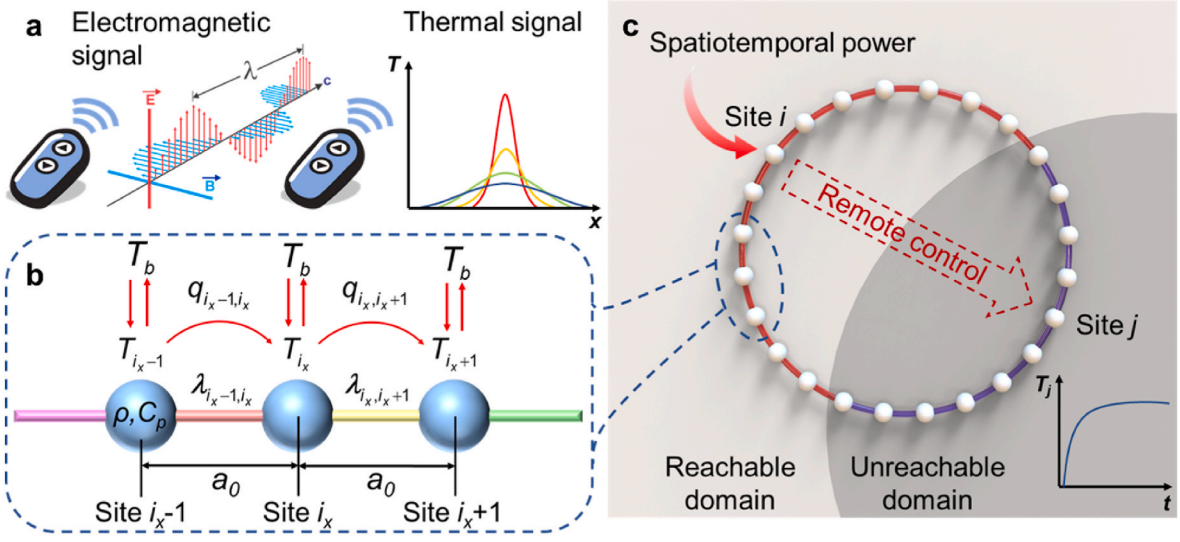

Fig. 1. Schematics for remote thermal control. (a) Schematic diagram for remote control of electromagnetic signal and thermal signal. (b) One-dimensional sphere-rod model of heat transfer process in thermal lattice. The spheres denote the site in thermal lattice, and the rods denotes coupling of neighboring sites. (c) Schematic representation for a general one-dimensional thermal lattice where spatiotemporal power is applied onto site i in reachable domain to control the local temperature of site j in unreachable domain. The inset picture denotes the temperature evolution of site j.

Then the time evolution of all the excess temperatures $\boldsymbol{\theta}(t) = [\theta_1(t), \theta_2(t), \ldots, \theta_N(t)]^{\dagger}$ in this system can be formally reformulated in matrix form

$$\partial_t \boldsymbol{\theta}(t) = -i\widehat{\boldsymbol{H}}\cdot\boldsymbol{\theta}(t), \tag{5}$$

where $\widehat{\boldsymbol{H}}$ indicates the governing Hamiltonian of the thermal lattice with $\widehat{\boldsymbol{H}}_{i_x,i_x} = -\left(D_{i_x-1,i_x} + D_{i_x,i_x+1} + C_{i_x}\right)$, $\widehat{\boldsymbol{H}}_{i_x-1,i_x} = D_{i_x-1,i_x}$ and $\widehat{\boldsymbol{H}}_{i_x,i_x+1} = D_{i_x,i_x+1}$. By inserting N equations analogous to Eq. (4) to Eq. (5), the governing Hamiltonian $\widehat{\boldsymbol{H}}$ can be derived as

$$\widehat{\boldsymbol{H}} = -i\begin{bmatrix} D_{1,2}+D_{1,N}+C_1 & -D_{1,2} & 0 & \cdots & \cdots & 0 & -D_{1,N} \\ -D_{1,2} & D_{1,2}+D_{2,3}+C_2 & -D_{2,3} & \cdots & \cdots & \cdots & 0 \\ \vdots & \vdots & \ddots & \cdots & \cdots & \cdots & \vdots \\ \vdots & \vdots & -D_{i-1,i} & D_{i-1,i}+D_{i,i+1}+C_i & -D_{i,i+1} & \cdots & \vdots \\ \vdots & \vdots & \vdots & \vdots & \ddots & \cdots & \vdots \\ 0 & \vdots & \vdots & \vdots & -D_{N-2,N-1} & D_{N-2,N-1}+D_{N-1,N}+C_N & -D_{N-1,N} \\ -D_{1,N} & 0 & \cdots & \cdots & 0 & -D_{N-1,N} & D_{N-1,N}+D_{1,N}+C_N \end{bmatrix}. \tag{6}$$

As only the nearreset neighoring interactions are considered in the sphere-rod model, the heat transfer process in the thermal lattice yields a tridiagonal $N \times N$ Hamiltonian. Note that the elements in $\widehat{\boldsymbol{H}}$ depend on the site geometry, thermophysical properties, and natural convection. Due to ciruclar boudnary condition as shown in Fig. 1(c) the $\widehat{\boldsymbol{H}}_{1,N}$ and $\widehat{\boldsymbol{H}}_{N,1}$ are nonzero. As all the elements in $\widehat{\boldsymbol{H}}$ are real numbers in our study, $\widehat{\boldsymbol{H}}$ describes the dissipative nature and is anti-Hermitian which is different from the Hamiltonian in quantum system [4]. If we inject spatiotemporal power $\boldsymbol{P}(t) = [P_1(t), \ldots, P_i(t), \ldots, P_N(t)]^{\dagger}$ onto the sites in the reachable domain, we can transform Eq. (5) as

$$\partial_t \boldsymbol{\theta}(t) = \widehat{\boldsymbol{M}}\cdot\boldsymbol{\theta}(t) + \boldsymbol{P}(t), \tag{7}$$

where $\widehat{\boldsymbol{M}} = -i\widehat{\boldsymbol{H}}$. By means of solving the PDE matrix, all the thermal states $\boldsymbol{\theta}(t) = [\theta_1(t), \theta_2(t), \ldots, \theta_N(t)]^{\dagger}$ at any given time t take the form as [34]

$$\boldsymbol{\theta}(t) = \boldsymbol{R}(0,t)\boldsymbol{\theta}_0 + \int_0^t \boldsymbol{R}(\tau,t)\boldsymbol{P}(\tau)d\tau, \tag{8}$$

where $\boldsymbol{R}$ represents the resolvent of Eq. (7) and $\boldsymbol{\theta}_0 = [\theta_1(0), \theta_2(0), \ldots, \theta_N(0)]^{\dagger}$ denotes the initial thermal state. Since the elements of $\widehat{\boldsymbol{H}}$ and $\widehat{\boldsymbol{M}}$ (i.e., thermophysical properties) are time-independent, heat transfer in the thermal lattice is reciprocal, thereby allowing the resolvent $\boldsymbol{R}$ to be simplified to the exponential matrix of $\widehat{\boldsymbol{M}}$ and thus designated as

$$\boldsymbol{R}(s,t) = \exp\left[\int_s^t \widehat{\boldsymbol{M}}(\tau)d\tau\right] = \exp[\widehat{\boldsymbol{M}}\cdot(t-s)]. \tag{9}$$

3. Remote control for thermal insulation

The first thermal targeting problem is to control the single-site temperature invariant with respect to time of site j in a system, i.e. $T_j(t)$ = constant, by means of either injecting an external power $P_{i\to j}(t)$ $(i \neq j)$ onto site i $\left[P_{i\to j}(t) > 0\right]$ or extracting the external power from site i $\left[P_{i\to j}(t) < 0\right]$, such that the command vector reads as $\boldsymbol{P}(t) = [0, \ldots, P_{i\to j}(t), \ldots, 0]^{\dagger}$. We designate the target time evolvement of temperature at site j as $T_j^{tg}(t)$ so that the target excess temperature is described as $\theta_j^{tg}(t) = T_j^{tg}(t) - T_b$ and introduce the following first kind Volterra integral equation

$$V_j(t) = \int_0^t \exp\left[\widehat{\boldsymbol{M}}\cdot(t-\tau)\right]_{ji} P_i(\tau)d\tau \tag{10}$$

in order to facilitate the calculation of the adequate required power control function at site i. According to Eq. (8), the relation between the Volterra integral equation and the heat transfer process of this system reads as

$$V_j(t) = \theta_j^{tg}(t) - \sum_k \exp\left(\widehat{\boldsymbol{M}}\cdot t\right)_{jk}\theta_{0k}. \tag{11}$$

The coupled solution of Eqs. (10) and (11) yields both the Volterra integral equation formulation $V_j(t)$ and the optimal external power control input $P_{i\to j}(t)$. Furthermore, the temporal evolution of the temperature at any untargeted spatial site x $(x \neq j \text{ or } i)$ is non-trivially modulated by the control intervention, as formally expressed through the constitutive relation:

$$\theta_x(t) = \sum_k \exp\left(\widehat{\boldsymbol{M}}\cdot t\right)_{xk}\theta_{0k} + \int_0^t \exp\left[\widehat{\boldsymbol{M}}\cdot(t-\tau)\right]_{xi} P_{i\to j}(\tau)d\tau, \tag{12}$$

where $\sum_k \exp\left(\widehat{\boldsymbol{M}}\cdot t\right)_{xk}\theta_{0k}$ characterizes the autonomous thermal evolvement at site x, governed by the self-consistent dynamics of the system in the absence of external control, quantified the intrinsic thermal coupling between adjacent sites and environmental interactions under equilibrium conditions T_b.

In addition, we further establish the necessary conditions required for maintaining thermal insulation at a specific site j. This constrained dynamic equilibrium is governed by the conservation law $\partial_t T_j^{tg}(t) = 0$ so that the time derivative of excess temperature at the target site j satisfies $\partial_t \theta_j^{tg}(t) = \partial_t\left[T_j^{tg}(t) - T_b\right] = 0$. The solution of this thermal insulation control problem can be rigorously derived by taking the temporal differentiation of Eq. (10) which couples the external power control to localized thermal dynamics. This derivation methodology yields the fundamental constraint equation for admissible power control, the Volterra integral equation of the second kind:

$$\partial_t V_j(t) = \int_0^t \widehat{\boldsymbol{M}}_{ji} \exp\left[\widehat{\boldsymbol{M}}\cdot(t-\tau)\right]_{ji} P_{i\to j}(\tau)d\tau + P_{i\to j}(t). \tag{13}$$

The central objective of thermal insulation at site j is mathematically achieved by performing time derivative on Eq. (11). This operational calculus yields a control-theoretic constraint that establishes the operator equivalence between the Volterra integral formalism of the second kind and the prescribed thermal insulation target at site j:

$$\partial_t V_j(t) = \partial_t \theta_j^{tg}(t) - \sum_k \widehat{\boldsymbol{M}}_{jk} \exp\left(\widehat{\boldsymbol{M}}\cdot t\right)_{jk}\theta_{0k}. \tag{14}$$

Next, we validate the above theoretical framework through numerical simulations and experimental measurements. We fabricate the aluminum circular ring (channel) with five circular disks with radius r = 2 cm (aluminum alloy 6063-T83 with thermal conductivity λ = 201 W/

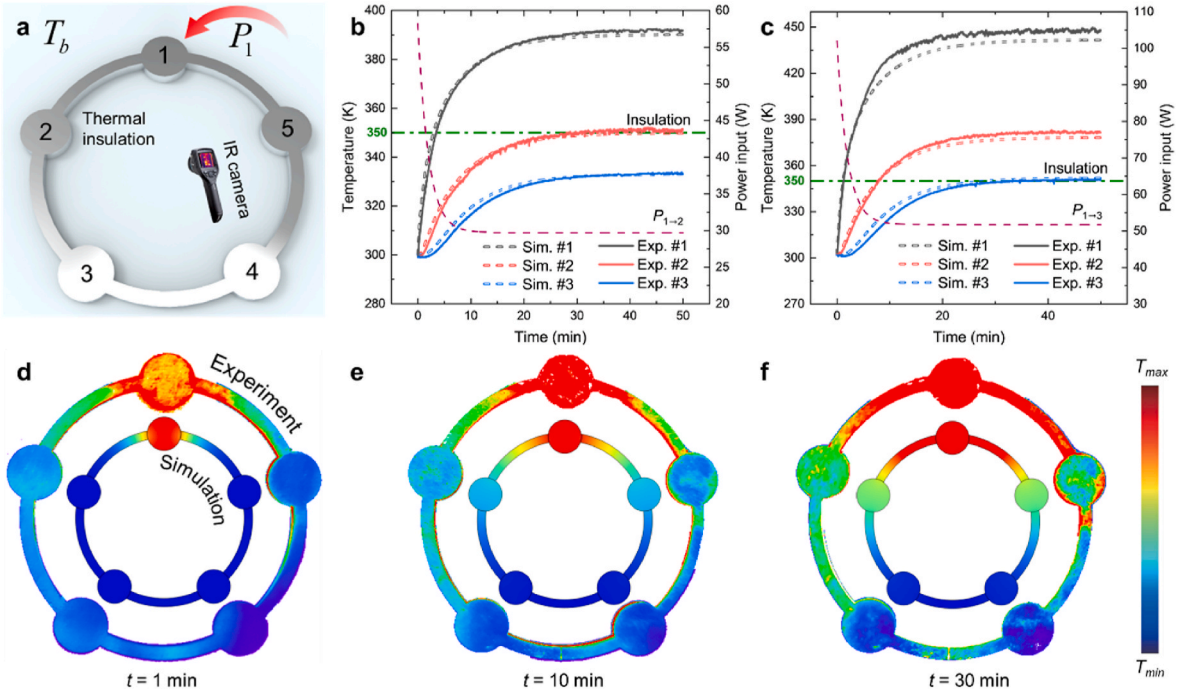

Fig. 2. Validation of thermal insulation via simulations and experiments. (a) Schematic for experimental setup of thermal insulation. The external power P_1 is injected onto site 1. A thermal camera is employed to observe the temperature evolutions in different sites. (b–c) Temperature evolutions at sites #1, #2 and #3 and the external powers $P_{1\to2}(t)$ and $P_{1\to3}(t)$ for thermal insulation at 350 K of site #2 (b) and site #3 (c), respectively. (d–f) Temperature fields in simulations and experiments at (d) $t = 1$ min, (e) $t = 10$ min and (f) $t = 30$ min for thermal insulation at site #2. Geometries in both simulations and experiments are the same while the experimental geometries are zoomed out for better comparative illustration.

(m-K), density $\rho = 2700$ kg/m^3 and heat capacity $C_p = 900$ J/(kg-K)) as shown in Fig. 2(a). The aluminum circular ring has the same geometric parameters with the lattice constant $a_0 = 12.5$ cm and the ring channel width $d = 1$ cm. The geometry is fabricated by wire electrical discharge machining with a fabrication tolerance of 0.2 mm. Given that all site surfaces are coplanar, radiative heat transfer between them is considered negligible. All these parameters were chosen according to the designed thermal diffusion coefficients, e.g., D_{i_x,i_x+1} between two disks i_x and $i_x + 1$. In the experiment, we use a thermoelectric heater controlled by PCB circuits to heat up the designed site, and employ a thermal infrared camera (FLIR T1010) and thermocouples (TE 3001) to measure the temperature evolutions.

The fabricated sample is embedded in an external bath at temperature $T_b = 300$ K, and the site temperatures of these disks are initially held at temperatures $T_1(0) = T_2(0) = T_3(0) = T_4(0) = T_5(0) = 300$ K unless specifically claimed hereinafter. The external command $P_1(t)$ is injected onto site #1 for different functionalities and the spatiotemporal power input is controlled by PCB control circuits. A thermoelectric heater is attached to site #1, with adjustable power according to the formula of $P_1(t)$. Finite element simulations are performed to numerically resolve the heat transfer process, encompassing heat conduction inside the lattice, heat convection with the external bath, and the input spatiotemporal power, thereby obtaining the spatiotemporal temperature fields to verify the experiments and theoretical framework.

As the first demonstration, we designate site 2 as the target thermally insulated domain with a fixed target temperature at 350 K, i.e., $T_2^{tg}(t) = 350$ K, and apply the appropriate time-dependent external power $P_{1\to2}(t)$ derived from Eqs. (13) and (14) onto site #1 for thermal insulation control. Due to geometry symmetry, the temperature evolutions of sites #2 and #5 will be the same, of sites #3 and #4 will be the same. As indicated in Fig. 2(b), the temperature evolutions at sites #1, #2 and #3 increases until reaching a plateau and the equilibrium temperature at site #2 (T_2) is 350 K, just as the designed target $T_2^{tg}(t) = 350$ K. Similarly, we can also designate site #3 as the target thermally insulated domain with $T_3^{tg}(t) = 350$ K and the optimal time-dependent external power input $P_{1\to3}(t)$ is applied onto site #1 in the same way. It is seen in Fig. 2 (c) that the temperature at site #3 increase first and saturate at 350 K eventually, which implies that we realize thermal insulation at site #3. Both the time-dependent external power inputs $P_{1\to2}(t)$ and $P_{1\to3}(t)$ are also shown in Fig. 2(b) and (c), respectively, and they are different for different target sites. The temperature field evolutions in both experiments and simulations at $t = 1$ min, 10 min and 30 min agree very well, as shown in Fig. 2(d)-2(f). It is seen that heat is transferred from site #1 to #3 and #4 in a symmetric way gradually with controllable temperatures at either #2 or #3, implying the accuracy and powerfulness of the aforementioned remote spatiotemporal control framework for thermal insulation.

4. Remote control for thermal synchronization

The proposed remote spatiotemporal control framework not only can be used to control a single-site local thermal state, but also can be applied to control multiple-site local thermal states. The second thermal targeting problem involves achieving temperature synchronization among multiple sites during transient relaxation process. To remove the geometry symmetry, we derive multiple optimal external commands to synchronize the temperature evolution of multiple targets. The simplest thermal synchronization problem is to find two external power controls $P_i(t)$ and $P_j(t)$ applied on sites i and j in this system in order to synchronize the temperature evolutions at two sites x and y $T_x(t)$ and $T_y(t)$ along the thermal relaxation. Therefore, the external command vector can be described as $\boldsymbol{P}(t) = [0, \ldots, P_i(t), \ldots, P_j(t), \ldots, 0]^{\intercal}$. We designate the target temporal excess temperature evolutions at sites x and y as $\boldsymbol{\theta}_{xy}^{tg}(t) = \left[\theta_x^{tg}(t) \quad \theta_y^{tg}(t)\right]^{\dagger}$ and it is straightforward to show that the appropriate power controls $\boldsymbol{P}_{ij}(t) = \left[P_i(t) \quad P_j(t)\right]^{\dagger}$ are solutions of the matrixial Volterra integral equation

$$\boldsymbol{V}_{xy}(t) = \int_0^t \begin{pmatrix} \boldsymbol{R}_{xi}(\tau,t) & \boldsymbol{R}_{xj}(\tau,t) \\ \boldsymbol{R}_{yi}(\tau,t) & \boldsymbol{R}_{yj}(\tau,t) \end{pmatrix} \boldsymbol{P}_{ij}(\tau)d\tau. \tag{15}$$

In accordance with Eq. (8), the relation between the matrixial Volterra integral equation and the heat transfer process of this system is recast as

$$\boldsymbol{V}_{xy}(t) = \boldsymbol{\theta}_{xy}{}^{tg}(t) - \sum_k \begin{pmatrix} \boldsymbol{R}_{xk}(0,t) \\ \boldsymbol{R}_{yk}(0,t) \end{pmatrix} \theta_{0k}. \tag{16}$$

By coupling Eqs. (15) and (16), both the Volterra integral equation formulation $\boldsymbol{V}_{xy}(t)$ and the optimal external power control input $\boldsymbol{P}_{ij}(t)$ can be derived. Furthermore, we establish the necessary conditions required for maintaining thermal insulation when the excess temperatures at sites x and y are synchronized, i.e., $\partial_t \boldsymbol{\theta}_{xy}^{tg}(t) = \partial_t \left[\theta_x^{tg} \quad \theta_y^{tg} \right]^\dagger = 0$. The solution of this thermal target control problem can be rigorously derived by taking the temporal differentiations of Eqs. (15) and (16). This derivation methodology yields the fundamental constraint equation for admissible power control, the Volterra integral equation of the second kind:

$$\partial_t \boldsymbol{\theta}_{xy}{}^{tg}(t) - \sum_k \begin{pmatrix} \widehat{\boldsymbol{M}}_{xk}\boldsymbol{R}_{xk}(0,t) \\ \widehat{\boldsymbol{M}}_{yk}\boldsymbol{R}_{yk}(0,t) \end{pmatrix} \theta_{0k} = \int_0^t \partial_t \begin{pmatrix} \boldsymbol{R}_{xi}(\tau,t) & \boldsymbol{R}_{xj}(\tau,t) \\ \boldsymbol{R}_{yi}(\tau,t) & \boldsymbol{R}_{yj}(\tau,t) \end{pmatrix} \boldsymbol{P}_{ij}(\tau)d\tau + \boldsymbol{P}_{ij}(\tau). \tag{17}$$

In order to observe the thermal synchronization, we put the experimental sample in an external thermal bath at temperature $T_b = 300\ K$ and all the local thermal states are initially at temperatures $T_1(0) = T_2(0) = T_3(0) = T_4(0) = 300$ K and $T_5(0) = 350$ K. We designate sites #3 and #5 as the target thermally synchronized domain, i.e., $T_3^{tg}(t) = T_5^{tg}(t) = 350$ K and apply the appropriate external power controls $P_1(t)$ and $P_2(t)$ derived from Eqs. (15) and (16). As indicated in Fig. 3(b), the temperature evolution at site #5 decreases first and then increases gradually with a plateau at 350 K, while the temperature evolution at site #3 gradually increases and saturates at 350 K. This is due to the different initial conditions at sites #3 and #5. Both the temperatures at site #3 and #5 are the same eventually, validating the thermal synchronization of the local thermal states at target sites. Besides, both the time-dependent $P_1(t)$ and $P_2(t)$ are also shown in Fig. 3(b). The simulated and experimental temperature fields at $t = 1$ min, 10 min and 30 min agree very well in Fig. 3(c)-3(e). It is seen that at the beginning, the temperature at site #5 is highest due to the initial condition. As time elapses, heat is transferred in the system with external commands injected onto sites #1 and #2 in an asymmetric way, and eventually achieves the similar temperatures at sites #3 and #5, implying the accuracy and efficacy of the aforementioned remote spatiotemporal control framework in thermal synchronization.

5. Remote control for thermal fluctuation

The previous thermal insulation and synchronization aims at controlling the target sites at constant temperature, and the third thermal targeting problem is to control the target temperature with fluctuational property. As the first attempt of thermal fluctuational control, we designate site #2 as the target fluctuational controlled domain, i.e., $T_2^{tg}(t) = 350 + 4\sin(1.2t + 0.8)$ K and the external power command $P_1(t)$ derived from Eqs. (10) and (11) is injected onto site #1. As illustrated in Fig. 4(a), due to the fluctuation properties of the target temperature (purple dash line), all the temperatures at different sites are fluctuated.

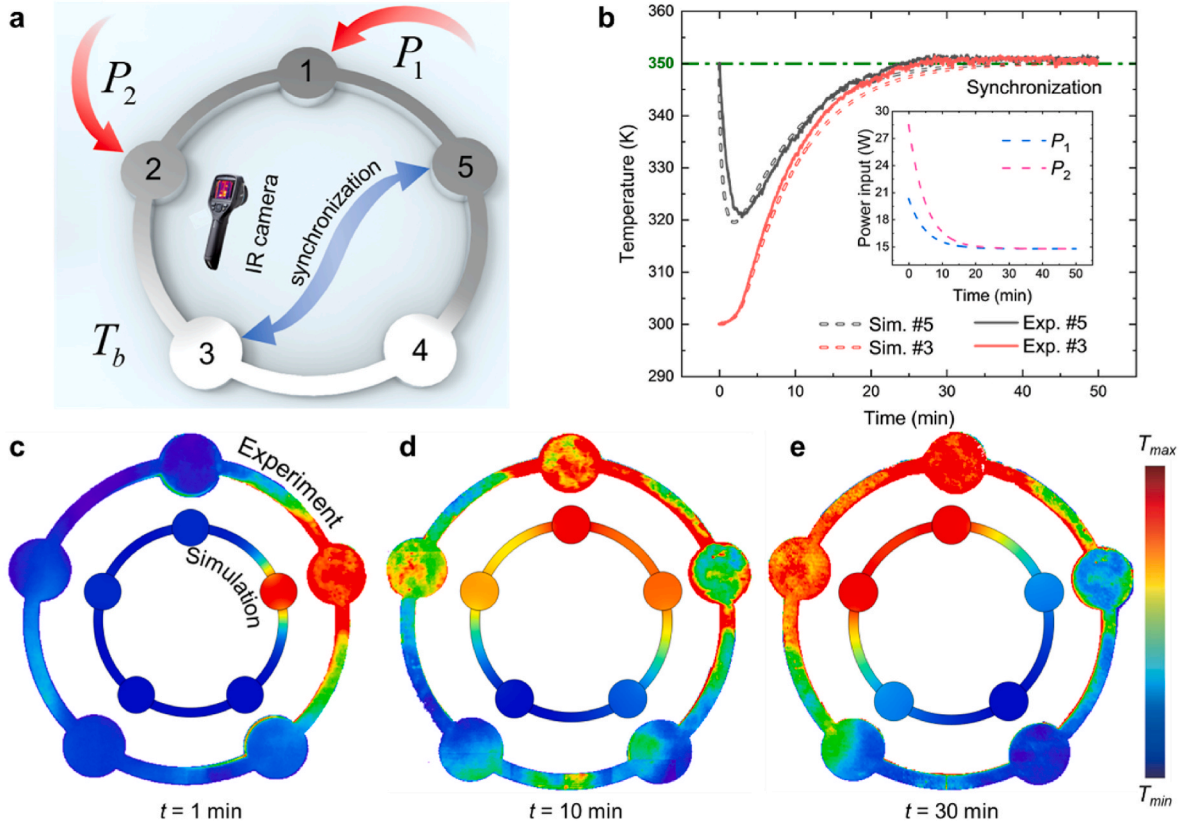

Fig. 3. Validation of thermal synchronization via simulations and experiments. (a) Schematic for experiment setup of thermal synchronization. The external powers P_1 and P_2 are injected onto site #1 and #2, respectively. A thermal camera is employed to observe the temperature evolutions in different sites. (b) Temperature evolutions at sites #3 and #5 and the external powers for thermal synchronization. (c–e) Temperature fields of simulations and experiments at (c) $t = 1$ min, (d) $t = 10$ min and (e) $t = 30$ min. Geometries in both simulations and experiments are the same while the experimental geometries are zoomed out for better comparative illustration.

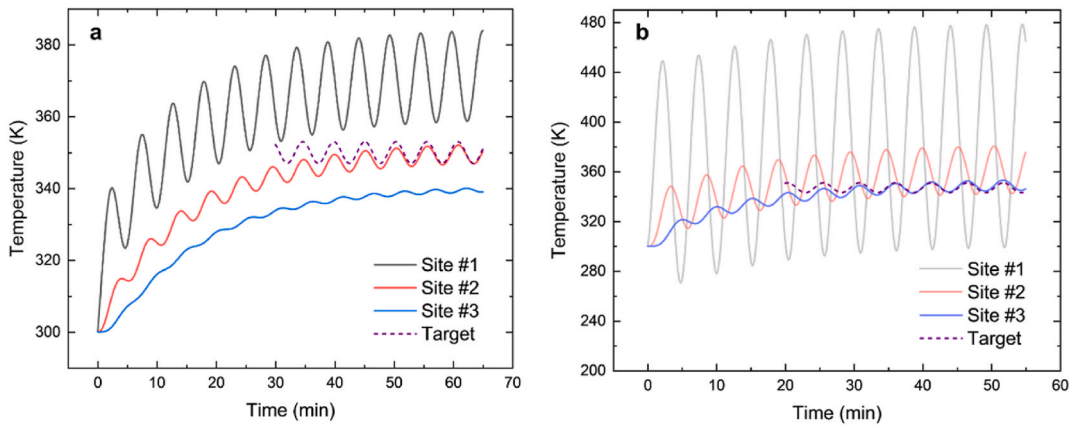

Fig. 4. Validation of thermal fluctuational control at a single site. (a) Temperature evolution of thermal states when site #2 is the target site with $T_2^{tg}(t) = 350 + 4\sin(1.2t + 0.8)$ K. (b) Temperature evolution of thermal states when site #3 is the target site with $T_3^{tg}(t) = 350 + 4\sin(1.2t + 2.3)$ K.

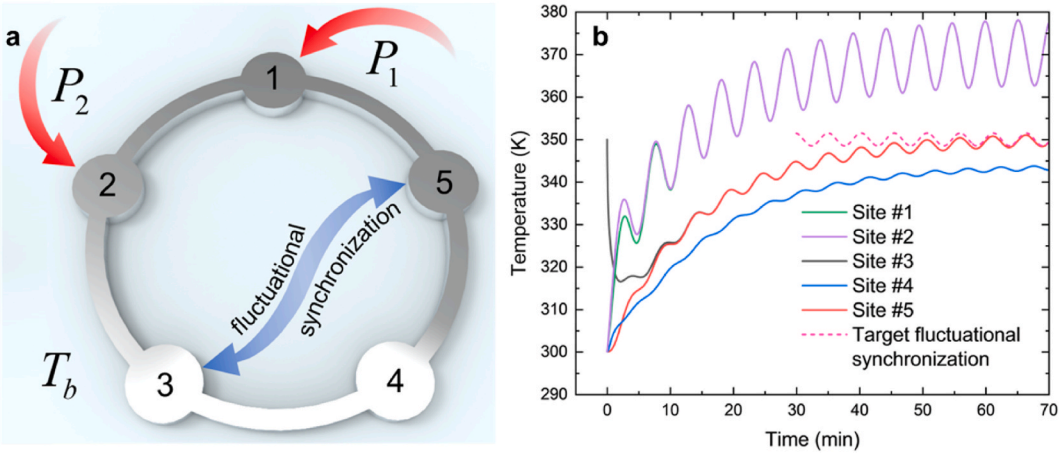

Fig. 5. Validation of thermal fluctuational control at multiple sites. (a) Schematic representation for setup of fluctuational synchronization control. The external power command P_1 and P_2 are injected onto sites #1 and #2 in order to realize thermal fluctuational synchronization at sites #3 and #5. (b) Temperature evolutions at all thermal sites and the temperature overlap at sites #3 and #5 implying the prescribed target fluctuational synchronization function.

Similar to Fig. 2(b), the temperature evolution at site #2 gradually increases but fluctuates after the fluctuated external power command $P_1(t)$ is injected. After $t = 30$ min, the temperature evolution at site #2 (red solid line) gradually coincides with the prescribed target temperature (purple dashed line). Then, we designate site #3 as the target fluctuational controlled domain, i.e., $T_3^{tg}(t) = 350 + 4\sin(1.2t + 2.3)$ K and the external power command $P_1(t)$ is injected onto site #1. Likewise, as presented in Fig. 4(b), the temperature evolution at site #3 (blue solid line) gradually coincides with the target fluctuational temperature (purple dashed line) after the external power command $P_1(t)$ is injected. It is worthy of mention that the temperature fluctuations at site #1 in Fig. 4(a) and (b) are largest in order for the temperature fluctuations to be transmitted to site #3.

As the second attempt of thermal fluctuational control, we perform required external power command onto two sites to achieve target fluctuational synchronization at another two sites. We designate site #3 and site #5 as the target fluctuational synchronization sites, i.e., $T_3^{tg}(t) = T_5^{tg}(t) = 350 + 1.5\sin(1.2t + 3.5)$ K. The external power command $P_1(t)$ and $P_2(t)$ are injected onto site #1 and site #2 respectively to achieve fluctuational control so that the temperature evolutions of the target site #3 and site #5 converge to our prescribed thermal target fluctuational synchronization control as denoted in Fig. 5(a). As illustrated in Fig. 5 (b), the temperature evolution at site #3 gradually decreases and then increases while the temperature evolution at site #5 is always increasing after the external power command $P_1(t)$ and $P_2(t)$ are injected. After $t = 30$ min, the temperature evolution at site #3 (black solid line) coincides with the temperature evolution at site #5 (red solid line) and then $T_3(t)$ and $T_5(t)$ gradually converge toward the target fluctuational synchronization temperature (pink dashed line) and fluctuates.

6. Conclusion

In summary, we propose a general protocol for remote spatiotemporal control of local temperature at the target sites in a thermal lattice. We construct the time-independent Hamiltonian of a thermal lattice system with consideration of conduction and convection simultaneously and derived the optimal external command to inject or extract power from the specific sites. Typical thermal functionalities, i.e., thermal insulation and thermal synchronization, are demonstrated theoretically, numerically, and experimentally. Besides, the remote control of thermal fluctuation is also demonstrated via fluctuation control. While the experiment is a five-site setup, the system can be significantly extended to more sites or two/three-dimensional scenarios. In our study, we assume linear heat conduction, invariant thermophysical properties, and neglect thermal radiation to derive the remote spatiotemporal control protocol, but the present protocol can be further adjusted to extend the application scenarios where these assumptions are broken. Moreover, the thermal lattice can be scaled if only the application can be modeled as sphere-rod model, and the temperature control precision need to be

re-evaluated. Of course, the local temperature may be controlled by mounting on-chip heaters/cooler with feedback electric circuit, but such traditional ways cannot be applied if the target sites are unreachable. Our study paves a new way for active thermal regulation via remote spatiotemporal control protocol and provide efficient alternatives for advanced thermal management in complex architectures.

CRediT authorship contribution statement

Quan Liu: Writing – original draft, Formal analysis, Conceptualization. **Zhaochen Wang:** Investigation, Conceptualization. **Sun-Kyung Kim:** Project administration. **Xiaobing Luo:** Investigation, Funding acquisition. **Philippe Ben-Abdallah:** Formal analysis. **Wonjoon Choi:** Project administration, Investigation. **Run Hu:** Writing – review & editing, Supervision, Funding acquisition, Conceptualization.

Declaration of competing interest

The authors declare that they have no conflicts of interest in this work.

Acknowledgements

The authors acknowledge the financial support from the National Key Research and Development Program of China [grant number 2022YFA1203104, 2024YFB4104701], National Natural Science Foundation of China [grant number 52422603, 52511540065, 52521008, 52161160332], Interdisciplinary Research Program of HUST [grant number 5003120094], Natural Science Foundation of Hubei Province [grant number 2023AFA072], Open Research Fund of Suzhou Laboratory [grand number SZLAB-1508-2024-TS016].

Data availability

Data will be made available on request.

References

[1] R. Messina, et al., Fluctuation-electrodynamic theory and dynamics of heat transfer in systems of multiple dipoles, Phys. Rev. B 88 (2013): 104307.
[2] S. Sanders, et al., Near-Field radiative heat transfer eigenmodes, Phys. Rev. Lett. 126 (2021): 193601.
[3] P. Ben-Abdallah, et al., Many-Body radiative heat transfer theory, Phys. Rev. Lett. 107 (2011): 114301.
[4] Z. Ren, et al., Terahertz metamaterials inspired by Quantum phenomena, Research 8 (2025) 597.
[5] J. Wang, et al., Coupling chiral cuboids with wholly auxetic response, Research 7 (2024) 463.
[6] H. Li, et al., One-Degree-of-Freedom mechanical metamaterials with arbitrary prescribability and rapid reprogrammability of force–displacement curves, Research 8 (2025) 715.
[7] S.-A. Biehs, et al., Near-field radiative heat transfer in many-body systems, Rev. Mod. Phys. 93 (2021): 025009.
[8] R. Ekeroth, et al., Anisotropic thermal magnetoresistance for an active control of radiative heat transfer, ACS Photonics 5 (2018) 705.
[9] S. Thongrattanasiri, et al., Complete optical absorption in periodically patterned Graphene, Phys. Rev. Lett. 108 (2012): 047401.
[10] R. Hu, et al., Illusion thermotics, Adv. Mater. 30 (2018): 1707237.
[11] Z. Zhu, et al., Inverse design of rotating metadevice for adaptive thermal cloaking, Int. J. Heat Mass Tran. 176 (2021): 121417.
[12] Z. Zhu, et al., Arbitrary-shape transformation multiphysics cloak by topology optimization, Int. J. Heat Mass Tran. 222 (2024): 125205.
[13] Z. Wang, et al., Inverse design of thermal metamaterials with holey engineering strategy, J. Appl. Phys. 132 (2022): 145102.
[14] C. Xia, et al., Broadband high optical transparent intelligent metasurface for adaptive electromagnetic wave manipulation, Research 7 (2024) 334.
[15] R. Hu, et al., Encrypted thermal printing with regionalization transformation, Adv. Mater. 31 (2019): 1807849.
[16] R. Hu, et al., Binary thermal encoding by energy shielding and harvesting units, Phys. Rev. Appl. 10 (2018): 054032.
[17] C.-X. Zhao, et al., Multiscale construction of bifunctional electrocatalysts for Long-Lifespan Rechargeable Zinc–Air batteries, Adv. Funct. Mater. 30 (2020): 2003619.
[18] S. Imhof, et al., Topolectrical-circuit realization of topological corner modes, Nat. Phys. 14 (2018) 925–929.
[19] R. Hu, et al., Thermal camouflaging metamaterials, Mater. Today 45 (2021) 120–141.
[20] W. Xi, et al., Ultrahigh-efficient material informatics inverse design of thermal metamaterials for visible-infrared-compatible camouflage, Nat. Commun. 14 (2023) 4694.
[21] T. Liu, et al., General three-dimensional thermal illusion metamaterials, Chin. Phys. B 33 (2024): 044401.
[22] M. Lei, et al., Reconfigurable, zero-energy, and wide-temperature loss-assisted thermal nonreciprocal metamaterials, Proc. Natl. Acad. Sci. 121 (2024): e2410041121.
[23] R. Ju, et al., Nonreciprocal heat circulation metadevices, Adv. Mater. 36 (2024): 2309835.
[24] D. Torrent, et al., Nonreciprocal thermal material by spatiotemporal modulation, Phys. Rev. Lett. 120 (2018): 125501.
[25] Y. Li, et al., Diffusive nonreciprocity and thermal diode, Phys. Rev. B 103 (2021): 014307.
[26] Y. Zhou, et al., Sustainable heat harvesting via thermal nonlinearity, Nat. Rev. Phys. 6 (2024) 769–783.
[27] Y. Li, et al., Heat transfer control using a thermal analogue of coherent perfect absorption, Nat. Commun. 13 (2022) 2683.
[28] Z. Liu, et al., Higher-Order topological In-Bulk corner State in pure diffusion systems, Phys. Rev. Lett. 132 (2024): 176302.
[29] Q. Liu, et al., Dynamically adjustable topological edge states in thermal diffusion-advection system, Fundam. Res. (2025), https://doi.org/10.1016/j.fmre.2025.02.001.
[30] Z. Wang, et al., Periodicity Alters Topological States in Thermal Diffusion System *Int J Heat Mass Tranf*, vol. 235, 2024: 126182.
[31] G. Xu, et al., Observation of bulk quadrupole in topological heat transport, Nat. Commun. 14 (2023) 3252.
[32] S. Yang, et al., Hierarchical bound states in heat transport, Proc. Natl. Acad. Sci. 121 (2024): e2412031121.
[33] G. Xu, et al., Configurable phase transitions in a topological thermal material, Phys. Rev. Lett. 127 (2021): 105901.
[34] P. Ben-Abdallah, A. Rodriguez, Controlling local thermal States in classical many-body systems, Phys. Rev. Lett. 129 (2022): 260602.